

An efficient approach to extract parameters from star cluster CMDs: *fitCMD*

Charles Bonatto

*Departamento de Astronomia, Universidade Federal do Rio Grande do Sul, Av. Bento Gonçalves 9500
Porto Alegre 91501-970, RS, Brazil*

4 August 2021

ABSTRACT

This work presents an approach (*fitCMD*) designed to obtain a comprehensive set of astrophysical parameters from colour-magnitude diagrams (CMDs) of star clusters. Based on initial mass function (IMF) properties taken from isochrones, *fitCMD* searches for the values of total (or cluster) stellar mass, age, global metallicity, foreground reddening, distance modulus, and magnitude-dependent photometric completeness that produce the artificial CMD that best reproduces the observed one; photometric scatter is also taken into account in the artificial CMDs. Inclusion of photometric completeness proves to be an important feature of *fitCMD*, something that becomes apparent especially when luminosity functions are considered. These parameters are used to build a synthetic CMD that also includes photometric scatter. Residual minimization between the observed and synthetic CMDs leads to the best-fit parameters. When tested against artificial star clusters, *fitCMD* shows to be efficient both in terms of computational time and ability to recover the input values.

Key words: (*Galaxy:*) open clusters and associations: general

1 INTRODUCTION

A colour-magnitude diagram (CMD) can be considered as the observational counterpart - on a purely photometric parameter space - of a stellar population (of given age and metallicity) whose individual masses are distributed according to an initial mass function (IMF). Over time, the mass-dependent stellar evolution changes the colour and magnitude of each star, thus leading to variations in the evolutionary sequences morphology. This reasoning implies that the CMD morphology encapsulates fundamental properties related to the star cluster itself, such as the stellar mass, age, metallicity, distance and reddening, among others.

The derivation of fundamental parameters of star clusters - in different dynamical states and formed in different environments - is important for a wide variety of studies, ranging from determination of the star-formation rate in the Galaxy (e.g. Lamers & Gieles 2006; Bonatto & Bica 2011) to investigations on the *infant mortality* (e.g. Lada & Lada 2003; Goodwin & Bastian 2006) and the dynamical state and cluster dissolution time scales (e.g. Goodwin 2009; Lamers et al. 2010), among others. Broadly speaking, photometry is the easiest - and cheapest - way to collect data on substantial fractions of a star cluster's population. Transported to CMDs, the collected data then can be used to try and

characterize the stellar population by extracting (some of) its fundamental parameters.

However, the combination of limited photometric depth with distances in excess of a few Kpc usually prevents the fainter stars from being detected by most of the available large-scale photometric surveys, thus producing partially-sampled CMDs that, in turn, may lead to a deficient derivation of cluster parameters. Besides, the presence of unknown fractions of binaries, differential reddening (especially for the very young clusters), and photometric scatter and completeness, also add complications to the task of using CMDs to derive cluster parameters. In particular, while age, distance and reddening can be relatively easy to estimate even in CMDs that are somewhat noisy and do not contain the fainter stars, metallicity, and especially mass, remain way more elusive to measure.

Considering the potentially large scope that well-determined cluster parameters may have in the current Galactic astrophysics, several approaches have already been developed in order to circumvent the difficulties associated to the process of extracting fundamental parameters from CMDs, e.g. Naylor & Jeffries (2006), Da Rio et al. (2010), Stead & Hoare (2011), and Bonatto et al. (2012). A summary of these approaches can be found in Bonatto et al. (2012). These approaches have been designed to deal with

particular types of clusters and/or parameters, and some are not practical in terms of the required computational time.

The approach presented in [Bonatto et al. \(2012\)](#) included most of the relevant parameters (mass, age, star-formation spread, distance modulus, foreground and differential reddening, and binaries) that are expected to make up the CMDs of young clusters. In short, the idea was to find the parameters that produce a CMD that best reproduces the observed one. This was done by minimizing the residuals between the observed and simulated CMDs by means of a global optimization method that varied the parameters along the direction of the minimization. Although the approach was able to recover the input parameters for simulated CMDs, it required extremely long computational times when applied to actual star clusters. To minimise stochasticity, the approach worked with the average CMD of several mock clusters, each sharing the same set of parameters. Thus, the number of stars turned out to be very large, which in turn affected critically the computational time.

Based on lessons learned especially in [Bonatto et al. \(2012\)](#), a more efficient and comprehensive approach - *fitCMD* - to extract parameters from CMDs is here presented. Instead of working with mock star clusters, it is based on a mass function (of a given age, metallicity, and mass) displaced some distance from the Sun, and affected by reddening and photometric scatter. An additional feature is that now photometric completeness is also taken into account. It is shown to be efficient both in terms of computational time and recovery of input values from simulated CMDs. Similarly to [Bonatto et al. \(2012\)](#), the rationale involves the minimization of residuals between the simulated and observed Hess diagrams ([Hess 1924](#)).

This paper is organised as follows: Sect. 2 describes the approach; Sect. 3 discusses the efficiency of *fitCMD* in retrieving parameters from simulated CMDs; Sect. 4 discusses the application of *fitCMD* to actual CMDs of open clusters, a dwarf galaxy, and a globular cluster. Concluding remarks are given in Sect. 5.

2 THE APPROACH: *fitCMD*

The basic goal of *fitCMD* is to extract fundamental parameters of a star cluster by means of the photometric information contained in its observed CMD. The underlying principle is to find an artificial CMD that best reproduces the observed one; the set of input parameters is then assumed to be representative of the star cluster itself. The parameters included here are the total mass stored in stars (or cluster mass, M_{cl}), age (t_{age}), global metallicity (Z), foreground reddening (or colour excess, CE) and the apparent distance modulus (DM). Photometric completeness is also taken into account by means of a Fermi function. Completeness as a function of the magnitude m is described as $f_C(m) = 1/(1 + \exp[k_F(m - m_{TO})])$, where m_{TO} is the turnover magnitude ($f_C(m_{TO}) = 0.5$) and k_F controls the steepness of the descent. Strictly speaking, this formulation refers to the completeness (at magnitude m) relative to that of the brightest stars. The analytical shape of the Fermi function appears to be convenient to describe the photometric completeness because it changes rather slowly at the bright end, and falls off exponentially after some fainter

magnitude. When completeness effects are irrelevant, the stellar density over the evolutionary sequences of a stellar population on a CMD should follow approximately that of a mass function. However, completeness artificially decreases the stellar density towards fainter magnitudes, and the comparison with the intrinsic density allows *fitCMD* to derive the completeness function parameters k_F and m_{TO} .

If binaries and differential reddening are ignored, an artificial star cluster CMD can be built by defining the following minimum set of parameters: M_{cl} , t_{age} , Z , CE and DM . Individual stellar masses are attributed according to an initial mass function (IMF), which can be chosen either as that of [Salpeter \(1955\)](#) or the segmented distribution of [Kroupa \(2001\)](#). Photometric scatter must also be added for more realism. In addition, a mass to light relation (MLR) - usually taken from isochrones - is required to produce the CMD representation of a mock star cluster. Examples of such experiments are in, e.g. [Bonatto et al. \(2012\)](#).

Regarding isochrones, this work employs the latest PARSEC¹ v1.2S+COLIBRI PR16 ([Bressan et al. 2012](#); [Marigo et al. 2017](#)) models, although any other system having an adequate coverage in age, metallicity and stellar mass can be used. The present work employs filters that are part of the following photometric systems (i) [Bessell \(1990\)](#) & [Bessell & Brett \(1988\)](#) (filters B, V, J, and K), (ii) DECam (filters g and r), and (iii) WFC/ACS (filters F606W and F814W). These isochrones contain stars with masses larger than $0.1M_{\odot}$ and are computed for a scaled-solar composition, and follow the relation $Y = 0.2485 + 1.78Z$, where Y is the He content and Z is the total metallicity; the solar metal content is $Z_{\odot} = 0.0152$. They also include the pre-main sequence phase. For an adequate coverage in age, the following values are considered: 1 – 10 Myr (in steps of $\Delta t = 1$ Myr), 10 – 20 Myr ($\Delta t = 2$ Myr), 20 – 50 Myr ($\Delta t = 5$ Myr), 50 – 100 Myr ($\Delta t = 10$ Myr), 100 – 500 Myr ($\Delta t = 25$ Myr), 500 – 1000 Myr ($\Delta t = 50$ Myr), 1000 – 13500 Myr ($\Delta t = 250$ Myr). In terms of the metallicity Z , the sampling is: from $10^{-4} - 10^{-3}$ (steps of $\Delta Z = 10^{-4}$), and $10^{-3} - 3 \times 10^{-2}$ ($\Delta Z = 10^{-3}$). As a consequence of such a relatively high resolution in age and metallicity, the total number of isochrones is 3978, but smaller ranges can be considered as well (see below).

Consider an artificial star cluster (SC_O) characterized by the set of intrinsic parameters (M_{cl} , t_{age} , Z , IMF). Obviously, any other model star cluster built with the same parameters will be a twin representation of SC_O . But, given the statistical nature of the individual stellar masses distribution - and, to some extent, their colours and magnitudes, the corresponding CMD may end up presenting significant differences with respect to that of SC_O , especially for young and low-mass cases (e.g. [Bonatto et al. 2012](#)). However, the fundamental point here is that the IMF is the same in all cases. So, instead of the discrete - and stochastic - CMDs, the present approach is based on properties of the IMF itself; a brief description is sketched below.

The first step consists in defining the ranges in which the parameters (M_{cl} , t_{age} , Z , CE , DM) will be searched. This, in turn, also sets the actual number of isochrones to be dealt with. With the IMF, a CMD is built for each

¹ Downloadable from <http://stev.oapd.inaf.it/cgi-bin/cmd>

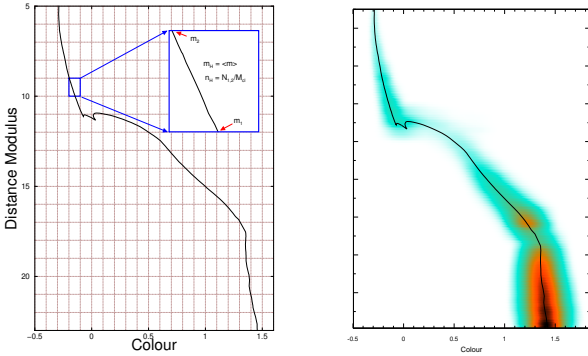


Figure 1. Left panel: given an IMF (represented by an isochrone), a CMD cell will contain $N_{1,2}$ stars with mass in the range (m_1, m_2) , with an average stellar mass $\langle m \rangle$; the stellar density is defined as $n_H = N_{1,2}/M_{cl}$. Right: Hess diagram - with photometric scatter added - of the CMD at left.

isochrone (at $DM = 0$ and no reddening), with a discretization in the colour/magnitude plane also defined at the beginning. So, a given CMD cell - containing stars with mass in the range (m_1, m_2) - will have the number of stars per cluster mass $n_H = N_{1,2}/M_{cl}$, as well as the average mass $\langle m \rangle$, which basically involves integrating the mass function ($\phi(m) = dN/dm$) between (m_1, m_2) : $N_{1,2} = \int_{m_1}^{m_2} \phi(m) dm$. This operation is done a single time and before the parameter search, which drastically reduces the computational time. After these procedures, each CMD cell will contain the respective relative density (number per cluster mass) of occurrence of stars, which is equivalent to the classical Hess diagram; hereafter, these diagrams are denoted by $H_M = H_M(M_{cl}, t_{age}, Z)$. This process is illustrated in Fig. 1. The same discretization is then applied to the observed star cluster CMD when building the respective Hess diagram. Photometric uncertainties are explicitly taken into account in the observed Hess diagram (e.g. Bonatto et al. 2012).

Photometric scatter is another key component of any artificial CMD that is expected to reproduce that of a star cluster. Consider the rows corresponding to the magnitude in the observed Hess diagram. For each row we compute the total stellar density and build the corresponding distribution function as a function of colour (columns). To minimize local fluctuations, the stellar density function for row N is actually the average of those in rows $N - 1$, N and $N + 1$. After identifying the colour where the maximum occurs, we compute the fraction of the total stellar density that each colour cell contains, both for bluer and redder colours with respect to the maximum. This broadening function is then applied to the respective row (magnitude value) in the simulated Hess diagram (see below). Thus, *fitCMD* allows both for colour-asymmetric and magnitude-dependent scatter. Comparisons of the actual photometric scatter with the simulated ones can be seen in Figs. 2-4.

The parameter search consists on finding the absolute minimum of the residual hyper-surface (R_H) defined as $R_H = (H_{obs} - H_{sim})^2$, where H_{obs} is the observed Hess

diagram and $H_{sim} = H_{sim}(M_{cl}, t_{age}, Z, CE, DM, k_F, m_{TO})$ is the simulated one. The values of M_{cl} , t_{age} , Z , CE , DM , k_F , and m_{TO} at the absolute minimum are assumed to represent those of the star cluster. In practical terms, locating the minima of R_H is equivalent to finding the parameters that minimize the quantity

$$S_R = \sum_{mag, col} W(mag) \times R_H(mag, col),$$

on the colour/magnitude plane. The sum runs over all Hess cells and $W(mag)$ is the statistical weight of each cell. $W(mag)$ corresponds to the inverse of the observed Hess density computed at the respective magnitude of each cell, i.e. $W(mag) = 1/\sum_{col} H_{obs}(mag, col)$.

We employ the global optimisation method known as Simulated Annealing (SA, Goffe et al. 1994). Simulated annealing originates from the metallurgical process by which the controlled heating and cooling of a material is used to increase the size of its crystals and reduce their defects. If an atom is stuck to a local minimum of the internal energy, heating forces it to randomly wander through higher energy states. In the present context, a state is the surface $R_H = R_H(M_{cl}, t_{age}, Z, CE, DM, k_F, m_{TO})$, corresponding to a specific set of values of the parameters being optimised. The slow cooling increases the probability of finding states of lower energy than the initial one. SA is a global optimisation technique that can escape from local minima (Goffe et al. 1994; Bonatto et al. 2012).

SA is an iterative and statistical technique that, at any given step k , randomly selects a new set of parameters (M_{cl}^k , t_{age}^k , Z^k , CE^k , DM^k , k_F^k , m_{TO}^k) from the respective ranges. This also means that the corresponding diagram $H_M^k = H_M(M_{cl}^k, t_{age}^k, Z^k)$ will be the only one to be used in this particular iteration. The cells of H_M^k are then multiplied by M_{cl}^k (to end up containing the number density of stars - same as H_{obs}), and shifted by the values of DM^k and CE^k . Finally, the artificial stellar density of each cell is decreased according to the photometric completeness of the corresponding magnitude, and photometric scatter is added (see above). What results is the diagram H_{sim} , from which R_H is built. As S_R decreases - i.e., a new minimum is found, SA concentrates on smaller parameter ranges, centred around the most promising values, and a new step ($k + 1$) is taken. Iterations stop when SA meets the convergence criterion: 5 consecutive repetitions of the same value of S_R . Typical runtimes are around 1 min on an *Intel Core i7 920@2.67 GHz* processor. However, given the statistical nature of SA, *fitCMD* should be repeated a few times to minimize the probability of getting stuck into a deep, but secondary minimum.

An interesting aspect of *fitCMD* is that, if the mass distribution of a cluster follows relatively closely a MF, the cluster mass should be retrievable quite well even when working with CMDs not severely truncated by limited photometric depth. In other words, if the age, metallicity, distance modulus and colour excess are reasonably well determined, the ratio observed/artificial Hess cells content - in any magnitude range - corresponds to M_{cl} .

Table 1. Recovery of model parameters

Range (mag) (1)	N (stars) (2)	M_{cl} (M_{\odot}) (3)	t_{age} (Gyr) (4)	$(m - M)_V$ (mag) (5)	$E(B - V)$ (mag) (6)	Z/Z_{\odot} (7)	M_{CMD} (M_{\odot}) (8)
Model	61034	20000	5	10.94	0.30	1.18	20000
Full	61034	20000 ⁺⁶⁴² ₋₅₉₈	5.0 ^{+0.3} _{-0.4}	10.94 ^{+0.03} _{-0.03}	0.30 ^{+0.01} _{-0.01}	1.18 ^{+0.02} _{-0.04}	20000
$V < 20$	8643	20000 ⁺¹⁸⁷⁰ ₋₁₅₉₀	5.0 ^{+0.24} _{-0.17}	10.94 ^{+0.03} _{-0.02}	0.30 ^{+0.01} _{-0.0}	1.18 ^{+0.04} _{-0.03}	7400
$V < 17$	3630	20500 ⁺²⁶⁴⁰ ₋₂₃₀₀	5.2 ^{+0.2} _{-0.1}	10.84 ^{+0.03} _{-0.01}	0.27 ^{+0.01} _{-0.01}	1.32 ^{+0.05} _{-0.02}	3900
Model	3103	1000	5	10.94	0.30	1.18	1000
Full	3103	993 ⁺⁹⁸ ₋₈₄	4.8 ^{+1.0} _{-1.1}	10.89 ^{+0.09} _{-0.07}	0.30 ^{+0.01} _{-0.01}	1.25 ^{+0.07} _{-0.07}	990
$V < 20$	416	991 ⁺¹⁸⁴ ₋₁₄₅	4.8 ^{+0.4} _{-0.8}	10.93 ^{+0.05} _{-0.06}	0.30 ^{+0.01} _{-0.01}	1.18 ^{+0.12} _{-0.06}	360
$V < 17$	184	1010 ⁺²⁴⁴ ₋₁₃₂	5.0 ^{+0.2} _{-0.2}	10.94 ^{+0.06} _{-0.06}	0.31 ^{+0.02} _{-0.01}	1.05 ^{+0.04} _{-0.02}	190

Table Notes. Col. (1) - magnitude threshold considered; (2) - number of stars present in the CMD; (3) - derived cluster mass; (4) - age; (5) - distance modulus; (6) - colour excess; (7) - metallicity; (8) - stellar mass actually present in CMD.

3 TESTING *fitCMD* ON ARTIFICIAL CMDS

The efficiency of *fitCMD* in recovering input parameters is tested with simulated CMDs, built with pre-defined values of M_{cl} , t_{age} , Z , CE , and DM . Individual stellar masses are attributed according to Kroupa's IMF (Kroupa 2001) - for masses larger than $0.1 M_{\odot}$ - until the sum matches M_{cl} ; the respective magnitudes are taken from the PARSEC isochrone corresponding to t_{age} and Z . Typical photometric uncertainties (for the simulated distance from the Sun) are added for each band k (σ_k). For more realism, the final photometric values for each star in band k correspond to those in the isochrone (m_k) plus a displacement that is taken from a Gaussian distribution centred on m_k and having the standard deviation σ_k , thus emulating observational photometric scatter.

Colour-magnitude diagrams dealt with here correspond to the classical $V \times (B - V)$. For simplicity, we consider 2 models with identical age ($t_{age} = 5$ Gyr), apparent distance modulus ($(m - M)_V = 10.94$), colour excess ($E(B - V) = 0.3$) - thus corresponding to $d_{\odot} = 1$ kpc, and global metallicity ($Z/Z_{\odot} = 1.18$), but with very different masses ($M_{cl} = 2 \times 10^4 M_{\odot}$ and $M_{cl} = 1 \times 10^3 M_{\odot}$) and, consequently, number of stars present in the CMD. Effects of photometric depth on the recovered parameters are also considered (Table 1). At $d_{\odot} = 1$ kpc, the mass distribution would reach a magnitude limit of $V \lesssim 31$. Then, to emulate photometric depth, we also consider CMDs restricted to $V \leq 20$ and $V \leq 17$.

Results obtained by *fitCMD* can be seen in Fig. 2 and are quantified in Table 1. The first point is that *fitCMD* does recover the input values - within uncertainties - even for the severely depleted CMDs. As expected, the cluster mass determination does not depend on photometric depth and/or number of stars present in the CMD. Age and metallicity, on the other hand, are more sensitive, especially to the evolutionary sequence tightness, i.e., essentially the number of stars.

4 APPLICATION TO ACTUAL STELLAR SYSTEMS

After exploring the ability of *fitCMD* to recover input model parameters, we now apply it to CMDs of actual star clusters. For this we selected some OCs with photometry publicly available in Vizier², NGC 6791, NGC 188, NGC 2682, NGC 2635, NGC 5288, and NGC 2323. Some details and values of parameters recently derived for these OCs are provided below.

NGC 6791: BVR photometry from Montgomery et al. (1994). A recent review on properties on this old and relatively metal-rich OC is in Martinez-Medina et al. (2018). Some relevant parameters are an age in the range 6 – 8 Gyr, $[Fe/H] \approx +0.4$, $d_{\odot} \approx 4$ kpc, and $M_{cl} \sim 5000 M_{\odot}$.

NGC 188: BVI photometry from Sarajedini et al. (1999). The review by Hills et al. (2015) provides the following parameter ranges, $t_{age} = 5.8$ to 6.5 Gyr, $[Fe/H] = -0.77$ to $+0.125$, $(m - M)_V = 11.441$ to 11.525, and $A_V = 0.162$ to 0.236.

NGC 2682 (M67): BVR photometry from Yadav et al. (2008). Available parameters in the literature: $t_{age} \sim 4$ Gyr, $M_{cl} \sim 2000 M_{\odot}$ (Hurley et al. 2005), $[Fe/H] = 0.00 \pm 0.06$ (Heiter et al. 2014), $E(B - V) = 0.041 \pm 0.004$ (Taylor 2007).

NGC 2635: BVI photometry from Moitinho et al. (2006), which also provides the values $t_{age} \sim 600$ Myr, $E(B - V) = 0.35$, $d_{\odot} \sim 4$ kpc, and $Z \sim 0.004$.

NGC 5288: BVI photometry from Piatti et al. (2006), which also provides the values $t_{age} \sim 130$ Myr, $E(B - V) = 0.75$, $d_{\odot} = 2.1 \pm 0.3$ kpc, and $Z \sim 0.04$.

NGC 2323: JHK_S photometry from 2MASS Skrutskie et al. (2006); parameters in the literature are $t_{age} = 140 \pm 20$ Myr, $d_{\odot} = 115 \pm 20$ pc, $[Fe/H] = 0.00$, and $E(B - V) = 0.23 \pm 0.06$ (Cummings et al. 2016); $t_{age} = 140 \pm 20$ Myr, $d_{\odot} = 900 \pm 100$ pc, and $M_{cl} \sim 890 M_{\odot}$ (Amin & Elsanhoury 2017).

As a caveat, it is important to remark that, except for NGC 2323, the remaining OCs may contain varying fractions of field stars contaminating their CMDs, which may lead to extrinsic stellar-density differences between the observed

² <http://vizier.u-strasbg.fr/viz-bin/VizieR>

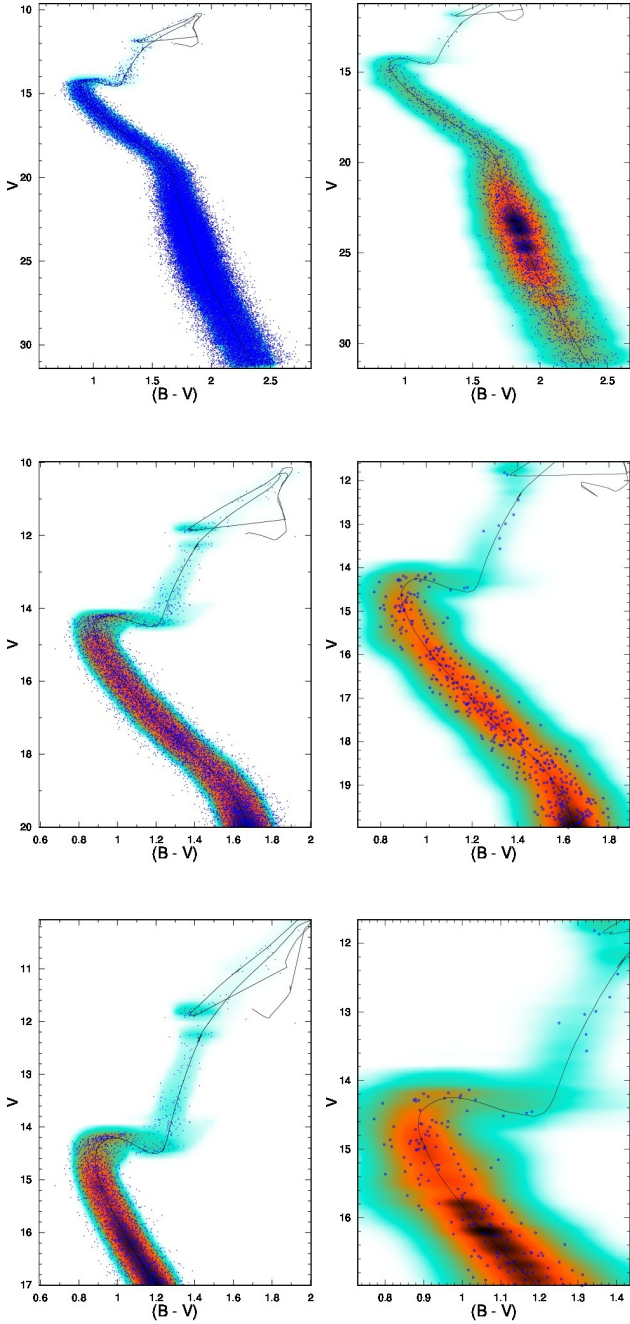


Figure 2. CMDs (blue dots) of simulated star clusters with $M_{cl} = 2 \times 10^4 M_{\odot}$ (left panels) and $M_{cl} = 1 \times 10^3 M_{\odot}$ (right). They are analysed by *fitCMD* over the full magnitude range (top panels), and partial ranges (middle and bottom). The best solutions are shown as Hess diagrams, in which the corresponding isochrone is set.

and IMF-simulated evolutionary sequences. The wide-field 2MASS photometry of NGC 2323 (obtained from VizieR) has been field-star cleaned with the decontamination algorithm described in Bonatto & Bica (2007), which employs a comparison field containing a statistically significant number of stars. Photometry for the other OCs, on the other hand, was obtained from specific observational projects, and usu-

ally corresponds to stars located within the cluster radius, thus with no comparison field available. Nevertheless, they provide interesting cases in which *fitCMD* can be tested under realistic conditions and those usually found in star clusters.

In all cases the age and metallicity parameters were allowed to vary over their whole ranges (Sect. 2); the remaining search parameters were also let to vary over broad ranges. For comparison reasons, simulations not taking photometric completeness into account were also performed and will be discussed later. The observed CMDs together with the respective *fitCMD* solutions are shown in Figs. 3-4; to minimize clutter, error bars are not shown in the cases where the OC has many stars. The best-fit and additional derived parameters are given in Table 2, among them is the stellar mass actually present in the CMD (M_{CMD}), which in some cases corresponds to a fraction of the total mass (M_{cl}).

Table 2. Parameters of selected open clusters derived with *fitCMD*

Cluster	M_{cl} ($10^3 M_{\odot}$)	age (Gyr)	$(m - M)_V$ (mag)	$E(B - V)$ (mag)	Z/Z_{\odot}	M_{CMD} (M_{\odot})	d_{\odot} (kpc)	M_{bol} (mag)	M_V (mag)	MLR $_{bol}$ (M_{\odot}/L_{\odot})	MLR $_V$ (M_{\odot}/L_{\odot})	k_F (13)	m_{TO} (mag) (14)
(1)	(2)	(3)	(4)	(5)	(6)	(7)	(8)	(9)	(10)	(11)	(12)	(13)	(14)
NGC 6791	10.2 ± 1.4	7.7 ± 0.4	$13.74^{+0.24}_{-0.08}$	0.27 ± 0.01	1.00 ± 0.05	1700	$3.74^{+0.41}_{-0.14}$	-5.0	-4.2	1.33	2.50	1.02 ± 0.15	20.2 ± 0.4
NGC 188	4.7 ± 0.5	6.3 ± 0.2	$11.41^{+0.12}_{-0.09}$	0.02 ± 0.01	1.58 ± 0.09	520	$1.86^{+0.10}_{-0.07}$	-4.2	-3.3	1.25	2.58	0.65 ± 0.10	16.4 ± 0.3
NGC 2682	1.9 ± 0.3	3.8 ± 0.2	$9.87^{+0.23}_{-0.08}$	0.13 ± 0.01	0.59 ± 0.04	390	$0.78^{+0.08}_{-0.03}$	-3.8	-3.2	0.70	1.18	1.06 ± 0.16	15.8 ± 0.3
NGC 2635	1.0 ± 0.2	0.28 ± 0.03	$14.77^{+0.82}_{-0.38}$	0.43 ± 0.02	0.53 ± 0.05	330	$4.72^{+1.77}_{-0.83}$	-4.9	-4.4	0.13	0.20	1.18 ± 0.18	19.6 ± 0.5
NGC 5288	0.8 ± 0.1	0.55 ± 0.04	$13.05^{+0.49}_{-0.28}$	0.67 ± 0.03	0.46 ± 0.05	310	$1.48^{+0.33}_{-0.19}$	-4.1	-3.8	0.23	0.29	6.40 ± 0.98	19.1 ± 0.5
NGC 2323	0.6 ± 0.1	0.32 ± 0.03	$9.74^{+0.21}_{-0.16}$	0.21 ± 0.03	0.99 ± 0.14	270	$0.81^{+0.08}_{-0.06}$	-4.1	-5.6	0.17	0.23	1.42 ± 0.22	15.2 ± 0.3

Table Notes. This table also gives the bolometric (col. 9) and absolute V (col. 10) magnitudes, the bolometric (col. 11) and V (col. 12) mass to light ratios; Fermi function parameters related to photometric completeness are in cols. (13) and (14).

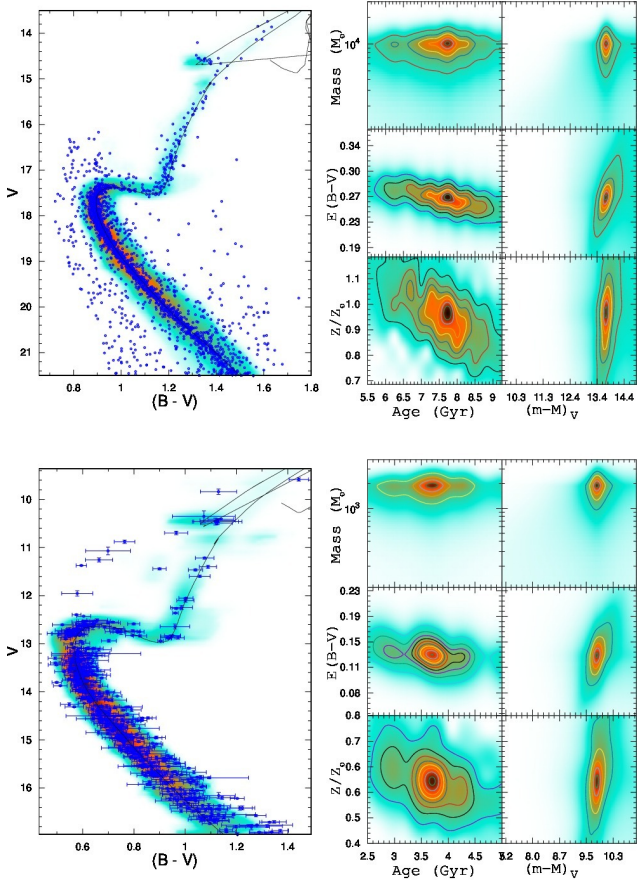


Figure 3. Left panels: same as Fig. 2 for the old OCs NGC 6791 (top) and NGC 2682 (bottom). The respective solution maps are shown in the right panels.

After finding the parameters corresponding to the absolute minimum of the R_H surface, their uncertainties are computed by means of the shape of the solution well in selected 2D projections (or solution maps). For instance, the solution map for mass and age is built by setting DM , Z , CE , k_F , and m_{TO} to their optimum values, while keeping M_{cl} and t_{age} free to vary within the pre-defined ranges. Uncertainties - usually asymmetric - are then computed based on properties (depth and width of the absolute minimum) of the solution map. Examples of solution maps are given in Fig. 3 for NGC 6791 and NGC 2682.

Besides the magnitude values as a function of mass, the PARSEC isochrones provide additional data that allow us to compute interesting star cluster integrated quantities, such as the bolometric and the absolute magnitude in the V band, and the mass-to-light ratio (MLR) both bolometric and in V (Tab. 2).

A few comments on the results obtained with *fitCMD* for the selected OCs. A direct comparison of all the output parameters from *fitCMD* with those in the literature cannot be done, since usually each work is aimed at a particular parameter (or restricted set of parameters). Nevertheless, the *fitCMD* ages agree - within the uncertainties - with those in the literature for NGC 6791, NGC 188 and NGC 2682, but differ somewhat for the remaining OCs. Con-

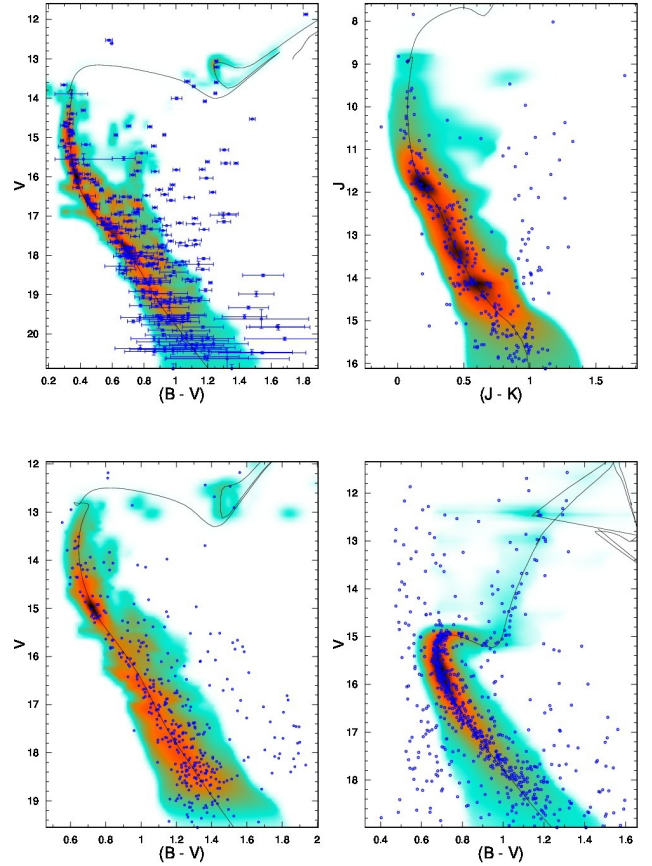


Figure 4. Same as Fig. 2 for NGC 2635 (top-left), NGC 2323 (top-right), NGC 5288 (bottom-left), and NGC 188 (bottom-right).

cerning M_{cl} , our values for NGC 2682 and NGC 2323 agrees with previous ones, but we find a value twice as large for NGC 6791. In summary, *fitCMD* provides values for a set of interesting astrophysical parameters obtained in a self-consistent way.

The 2 free parameters related to the photometric completeness are given in Tab. 2, and the completeness functions derived for the sample OCs are shown in Fig. 5. Among the selected OCs, NGC 188 is the one that suffers the highest degree of photometric completeness, beginning even at the brightest observed magnitude ($V \sim 11$ and $m_{TO} \approx 16.4$). NGC 5288, on the other hand, is the least affected, with completeness only affecting stars fainter than $V \sim 18$, with $m_{TO} \approx 19.1$.

Another way to examine the results is by comparing the observed luminosity function (LF) with that measured on the CMD built with the best-fit parameters (Fig. 6). The LFs are built by simply integrating the stellar density across the magnitude axis, thus implying that some contribution from contaminant stars may be present in the observed LFs. For a cleaner visualization, Fig. 6 shows the 1σ bounds of the observed LFs. In general, *fitCMD* reproduces the observed LFs, within the uncertainties, even at the faint end where completeness is more important. For comparison purposes, Fig. 6 also shows the LF produced by *fitCMD*

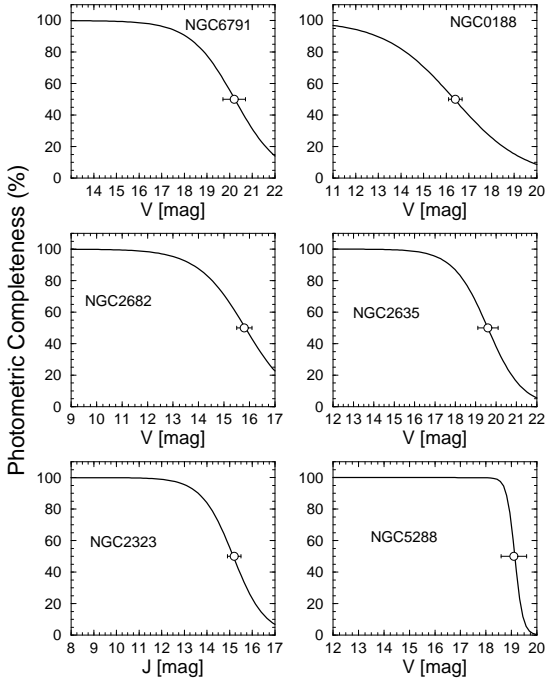


Figure 5. Photometric completeness (f_C) as a function of magnitude (m): $f_C(m) = 1/(1 + \exp[k_F(m - m_{TO})])$. Turnover magnitude (m_{TO}) is shown by the open circle.

when photometric completeness is not taken into account (red line). Significant deviations occur with respect to both the complete and observed LFs, especially at the faint magnitude ranges for the OCs most affected by completeness. This occurs because *fitCMD* tries to match the observed stellar density in all cells according to an IMF. Since photometric completeness naturally decreases the stellar densities (especially at the faint end of CMDs), *fitCMD* also lowers the stellar density in brighter cells. Finally, Fig. 6 shows the completeness-corrected LFs (blue line).

4.1 Special cases

After being applied to artificial and classical OCs, it would be interesting to check the performance of *fitCMD* on potentially more difficult cases. To this end, the Milky Way satellite Reticulum II and the globular cluster (GC) 47 Tuc have been selected. Both objects contain mixtures of stellar populations (see below) probably characterized by different ages and metallicities.

The dwarf galaxy Ret II (DES J0335.6-5403) was discovered by the Dark Energy Survey (DES; Bechtol et al. 2015). Parameters for Ret II derived by Bechtol et al. (2015) are the half-light radius $R_{hl} \approx 6'$, distance to the Sun $d_\odot = 32$ kpc, stellar mass $M_{cl} = (2.6 \pm 0.2) \times 10^3 M_\odot$, absolute magnitude $M_V = -3.6 \pm 0.1$, $age = 10 \pm 5$ Gyr, and the global metallicity $Z < 0.0003$. More recently, Mutlu-Pakdil et al. (2018)

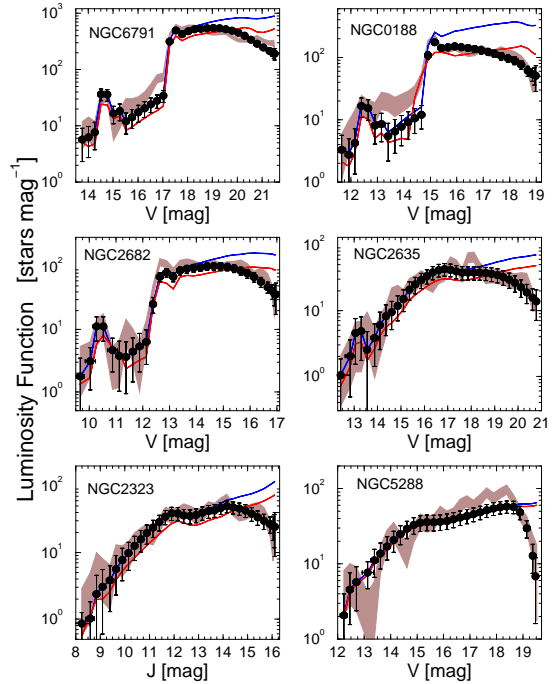


Figure 6. Luminosity functions. Shaded region: 1σ bounds of the observed LF; black symbols: *fitCMD* simulated LF; blue solid line: completeness-corrected LF; red line: best-fit LF without considering completeness.

studied Ret II with deep Magellan/Megacam photometry (also for stars within R_{hl}), finding $d_\odot = 31.4 \pm 1.4$ kpc, $M_V = -3.1 \pm 0.1$, $age = 13.5$ Gyr, and $[Fe/H] = -2.4$; for $0.0 < [\alpha/Fe] < 0.4$, the total metallicity of Ret II would be $Z < 0.0001$, consistent with the value derived by Bechtol et al. (2015).

Photometry for Ret II stars in g and r bands (corresponding to the DES system) has been obtained from the NOAO Data Lab³ in a region of $30'$ radius around its central coordinates, $RA(J2000) = 03^h 35' 49''$ and $DEC(J2000) = -54^\circ 02' 48''$. This setup was necessary in order to produce a field-stars decontaminated CMD by means of the Bonatto & Bica (2007) algorithm. For consistency and comparison purposes with both previous works, the region analyzed here corresponds to the area within R_{hl} . The decontaminated CMD together with the *fitCMD* solution are shown in Fig. 7. The corresponding *fitCMD* parameters are $M_{cl} = (2.7 \pm 0.5) \times 10^3 M_\odot$ (only $\approx 8\%$ of this mass is present on the observed CMD), $age = 13.0^{+0.3}_{-0.9}$ Gyr, $Z = 0.0002$, $d_\odot = 30.6 \pm 1.4$ kpc, the absolute magnitude in g $M_g = -3.2$, and the bolometric magnitude $M_{bol} = -3.72$. V magnitudes can be obtained from g and r by the transformation $V = g - 0.487(g - r) - 0.025$ (Bechtol et al. 2015), resulting in $M_V = -3.5$. Within the quoted uncertainties,

³ https://datalab.noao.edu/query.php?name=des_dr1.main

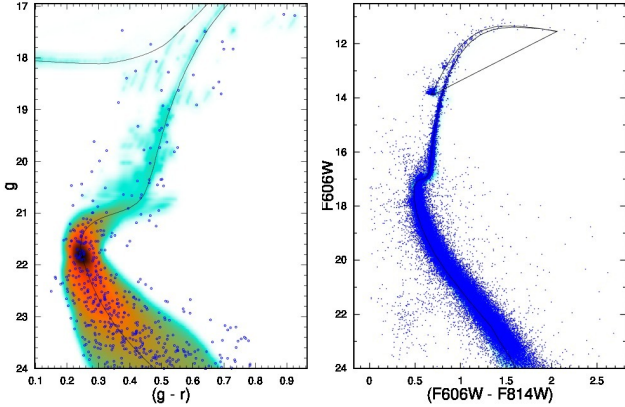


Figure 7. Left panels: same as Fig. 2 for the dwarf galaxy Ret II (left) and the GC 47 Tuc (right).

these parameters agree with the previous ones, except for the lower metallicity implied by Mutlu-Pakdil et al. (2018). Luminosity and photometric completeness functions are shown in Fig. 8. Consistently with ground-based observations of a distant object, Ret II photometry appears to be affected by completeness issues even at the bright end of the LF.

47 Tucanae (NGC 104) is the second brightest Milky Way GC after *Omega Centauri* (NGC 5139). Its tens of thousands stars distribute across $\sim 50'$ of the southern sky. 47 Tuc lies at $d_{\odot} \approx 4.5$ kpc from the Sun, displays a small and dense central core ($R_c \approx 0'.36$) and has half-light and tidal radii of $R_{hl} \approx 3.2'$ and $r_t \approx 43'$, respectively (Harris 2010). More recently, 47 Tuc was shown to host multiple stellar populations (Milone et al. 2012).

High-quality photometry for 47 Tuc is available as part of the HST WFC/ACS GC sample under program number GO 10775, with A. Sarajedini as PI. GO 10775 is a HST Treasury project in which 66 GCs were observed through the F606W and F814W filters with a field of view of $\approx 200'' \times 200''$ (Sarajedini et al. 2007). Working with this photometry, Wagner-Kaiser et al. (2017) found $A_V = 0.105 \pm 0.002$, $[Fe/H] = -0.72$ ($[\alpha/Fe] \approx +0.4$), which corresponds to $Z \approx 0.006$, and the rather old value $age = 13.494^{+0.006}_{-0.022}$ Gyr. On the other hand, working with deep WFC3 IR photometry, Correnti et al. (2016) derived $age = 11.6 \pm 0.7$ Gyr. It is clear that there is no consensus on the exact age of 47 Tuc. Indeed, Brogaard et al. (2017) find the value 11.8 Gyr, with lower and upper limits (3σ) at 10.4 and 13.4 Gyr, a range that appears to realistically represent the actual age uncertainty of 47 Tuc. Concerning the stellar mass of 47 Tuc, N-body computations of Marks & Kroupa (2010) provide $7 \times 10^5 M_{\odot}$, while analysis of central velocity dispersions coupled to fits of dynamical models by Kimmig et al. (2015) imply $(7 \pm 1) \times 10^5 M_{\odot}$.

The *fitCMD* analysis of 47 Tuc is based on the Sarajedini et al. (2007) photometry; as an additional quality constraint, only stars with photometric uncertainty lower than 0.1 mag in F606W and F814W (reducing to ≈ 128000 the number of available stars) are considered. The *fitCMD* solution for 47 Tuc is shown in Fig. 7, and the best-fit parameters are $M_{cl} = (3.4 \pm 0.4) \times 10^5 M_{\odot}$ ($\approx 24\%$ of this is on the observed CMD), $age = 12.0^{+0.3}_{-0.5}$ Gyr, $Z = 0.004$,

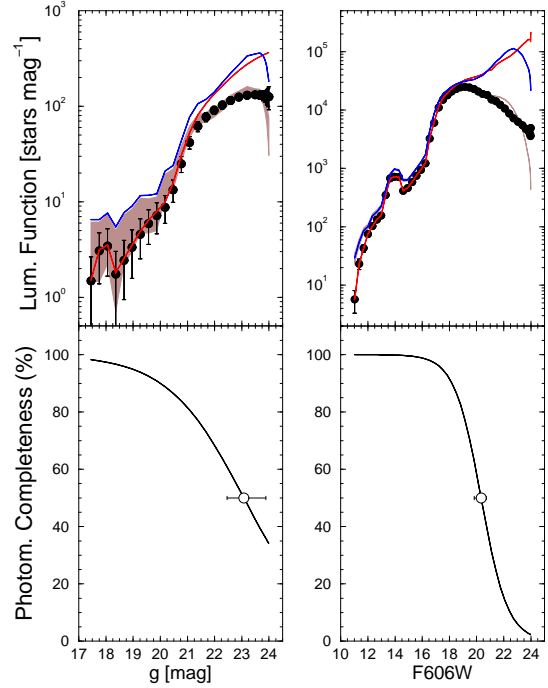


Figure 8. Top: same as Fig. 6 for Ret II (left) and 47 Tuc (right); bottom: same as Fig. 5.

$d_{\odot} = 4.5 \pm 0.1$ kpc, the absolute magnitude in F606W $M_{F606W} = -8.34$, the bolometric magnitude $M_{bol} = -8.63$, and $A_V = 0.11 \pm 0.01$. *fitCMD* age agrees quite well with the values of Brogaard et al. (2017) and Correnti et al. (2016). The *fitCMD* value for the mass corresponds to about half of the dynamical estimates (see above). However, it should be noted that the *fitCMD* value is based on the stars present in the area sampled by WFC/ACS, which has a radius corresponding to about half of R_{hl} . Interestingly, photometric completeness is inconspicuous for $F606W \lesssim 16$, but falls off quite steeply for $F606W \gtrsim 18$ (Fig. 8).

5 CONCLUDING REMARKS

fitCMD is an approach that extracts a set of astrophysical parameters from CMDs of star clusters. The rationale is to transpose theoretical IMF properties to their observational counterpart, the CMD. This requires finding values of the total (or cluster) stellar mass, age, global metallicity, foreground reddening, distance modulus, as well as for parameters describing magnitude-dependent photometric completeness. These parameters - including photometric scatter - are used to build a synthetic CMD that is compared with that of a star cluster. Residual minimization between observed and synthetic CMDs - by means of the global optimization algorithm Simulated Annealing - then leads to the best-fit parameters.

The efficiency of *fitCMD*, both in terms of computa-

tional time and ability to recover input parameters, has been tested with CMDs of artificial and observed star cluster - as well as of a dwarf galaxy and a globular cluster, with excellent results. In principle, *fitCMD* can be used with any isochrone set that provides magnitudes for at least 2 different bands for stellar masses covering as wide as possible a range. In addition, the isochrone set should also provide a comprehensive coverage - and resolution - both in age and metallicity.

ACKNOWLEDGEMENTS

Thanks to an anonymous referee for important comments and suggestions. This research has made use of the VizieR catalogue access tool, CDS, Strasbourg, France. This publication makes use of data products from the Two Micron All Sky Survey, which is a joint project of the University of Massachusetts and the Infrared Processing and Analysis Center/California Institute of Technology, funded by the National Aeronautics and Space Administration and the National Science Foundation. C.B. acknowledges support from the Brazilian Institution CNPq.

REFERENCES

- Amin M. Y., Elsanhoury W. H., 2017, *Serbian Astronomical Journal*, **194**, 59
- Bechtol K., et al., 2015, *ApJ*, **807**, 50
- Bessell M. S., 1990, *PASP*, **102**, 1181
- Bessell M. S., Brett J. M., 1988, *PASP*, **100**, 1134
- Bonatto C., Bica E., 2007, *MNRAS*, **377**, 1301
- Bonatto C., Bica E., 2011, *MNRAS*, **415**, 2827
- Bonatto C., Lima E. F., Bica E., 2012, *A&A*, **540**, A137
- Bressan A., Marigo P., Girardi L., Salasnich B., Dal Cero C., Rubele S., Nanni A., 2012, *MNRAS*, **427**, 127
- Brogaard K., VandenBerg D. A., Bedin L. R., Milone A. P., Thygesen A., Grundahl F., 2017, *MNRAS*, **468**, 645
- Correnti M., Gennaro M., Kalirai J. S., Brown T. M., Calamida A., 2016, *ApJ*, **823**, 18
- Cummings J. D., Kalirai J. S., Tremblay P.-E., Ramirez-Ruiz E., 2016, *ApJ*, **818**, 84
- Da Rio N., Gouliermis D. A., Gennaro M., 2010, *ApJ*, **723**, 166
- Goffe W. L., Ferrier G. D., Rogers J., 1994, *Journal of Econometrics*, **60**, 65
- Goodwin S. P., 2009, *Ap&SS*, **324**, 259
- Goodwin S. P., Bastian N., 2006, *MNRAS*, **373**, 752
- Harris W. E., 2010, preprint, ([arXiv:1012.3224](https://arxiv.org/abs/1012.3224))
- Heiter U., Soubiran C., Netopil M., Paunzen E., 2014, *A&A*, **561**, A93
- Hess R., 1924, *Probleme der Astronomie. Festschrift fur Hugo v. Seeliger.* (Berlin:Springer), p. 265
- Hills S., von Hippel T., Courteau S., Geller A. M., 2015, *AJ*, **149**, 94
- Hurley J. R., Pols O. R., Aarseth S. J., Tout C. A., 2005, *MNRAS*, **363**, 293
- Kimmig B., Seth A., Ivans I. I., Strader J., Caldwell N., Anderton T., Gregersen D., 2015, *AJ*, **149**, 53
- Kroupa P., 2001, *MNRAS*, **322**, 231
- Lada C. J., Lada E. A., 2003, *ARA&A*, **41**, 57
- Lamers H. J. G. L. M., Gieles M., 2006, *A&A*, **455**, L17
- Lamers H. J. G. L. M., Baumgardt H., Gieles M., 2010, *MNRAS*, **409**, 305
- Marigo P., et al., 2017, *ApJ*, **835**, 77
- Marks M., Kroupa P., 2010, *MNRAS*, **406**, 2000
- Martinez-Medina L. A., Gieles M., Pichardo B., Peimbert A., 2018, *MNRAS*, **474**, 32
- Milone A. P., et al., 2012, *ApJ*, **744**, 58
- Moitinho A., Carraro G., Baume G., Vázquez R. A., 2006, *A&A*, **445**, 493
- Montgomery K. A., Janes K. A., Phelps R. L., 1994, *AJ*, **108**, 585
- Mutlu-Pakdil B., et al., 2018, *ApJ*, **863**, 25
- Naylor T., Jeffries R. D., 2006, *MNRAS*, **373**, 1251
- Piatti A. E., Clariá J. J., Ahumada A. V., 2006, *MNRAS*, **367**, 599
- Salpeter E. E., 1955, *ApJ*, **121**, 161
- Sarajedini A., von Hippel T., Kozhurina-Platais V., Demarque P., 1999, *AJ*, **118**, 2894
- Sarajedini A., et al., 2007, *AJ*, **133**, 1658
- Skrutskie M. F., et al., 2006, *AJ*, **131**, 1163
- Stead J. J., Hoare M. G., 2011, *MNRAS*, **418**, 2219
- Taylor B. J., 2007, *AJ*, **133**, 370
- Wagner-Kaiser R., et al., 2017, *MNRAS*, **468**, 1038
- Yadav R. K. S., et al., 2008, *A&A*, **484**, 609